An Unbiased Proteomic Platform for Activity-based Arginylation Profiling

Zongtao Lin[1,*], Yixuan Xie[1], Joanna Gongora[1], Xingyu Liu[1], Emily Zahn[1], Bibhuti Bhusana Palai[1], Daniel Ramirez[1], Rick M. Searfoss[1], Francisca N. Vitorino[1], Geoffrey P. Dann[2], Chenfeng Zhao[3], Xian Han[1], Brittany MacTaggart[4], Xin Lan[5], Dechen Fu[5], Lina Greenberg[1], Yi Zhang[5], Kory J. Lavine[6], Michael J. Greenberg[1], Dongwen Lv[7], Anna Kashina[4], Benjamin A. Garcia[1,*]

[1]*Department of Biochemistry and Molecular Biophysics, Washington University in St. Louis, St. Louis, MO 63110*

[2]*Department of Biochemistry and Biophysics, University of Pennsylvania, Philadelphia, PA, 19104*

[3]*McKelvey School of Engineering, Washington University in St. Louis, St. Louis, MO 63110*

[4]*School of Veterinary Medicine, University of Pennsylvania, Philadelphia, PA 19104*

[5]*Department of Biochemistry, Case Western Reserve University, Cleveland, OH 44106*

[6]*Department of Medicine, Washington University School of Medicine, St. Louis, MO, USA*

[7]*Department of Biochemistry and Structural Biology, University of Texas Health Science Center at San Antonio, San Antonio, TX 78229*

Correspondence.* ***Email**: bagarcia@wustl.edu (B.A.G.), zongtao@wustl.edu (Z.L.),* ***Tel.****: 314-362-3085*

Abstract. Protein arginylation is an essential posttranslational modification (PTM) catalyzed by arginyl-tRNA-protein transferase 1 (ATE1) in mammalian systems. Arginylation features a post-translational conjugation of an arginyl to a protein, making it extremely challenging to differentiate from translational arginine residues with the same mass in a protein sequence. Here we present a general activity-based arginylation profiling (ABAP) platform for the unbiased discovery of arginylation substrates and their precise modification sites. This method integrates isotopic arginine labeling into an ATE1 assay utilizing biological lysates (*ex vivo*) rather than live cells, thus eliminating translational bias derived from the ribosomal activity and enabling *bona fide* arginylation identification using isotopic features. ABAP has been successfully applied to an array of peptide, protein, cell, patient, and animal tissue samples using 20 µg sample input, with 229 unique arginylation sites revealed from human proteomes. Representative sites were validated and followed up for their biological functions. The developed platform is globally applicable to the aforementioned sample types and therefore paves the way for functional studies of this difficult-to-characterize protein modification.

Keywords: arginylation, arginyltransferase, proteomics, posttranslational modification, protein profiling

Introduction

As a critical posttranslational modification (PTM), arginylation is catalyzed by arginyltransferase (ATE1) which is the only known enzyme capable of installing arginylation in mammalian systems. The absence of arginylation in ATE1 knockout (KO) models resulted in embryonic lethality due to heart defects in cardiovascular development and angiogenic remodeling[1]. Specifically, ATE1KO caused thinned myocardium with immature septa, non-separation of the aorta and pulmonary artery, resulting in defects in cardiac contractility, myofibril dysfunction and eventually embryonic death[1], demonstrating the essential nature of arginylation[1]. Tissue-specific knockdown (KD) or deletion (KO) of arginylation resulted in impaired myosin phosphorylation and thrombus formation[2], elevated myocardial fibrosis and progressive heart failure[3], cardiomyocyte hypertrophy[4], and many other symptoms[5,6]. At the molecular level, the arginylation field has long tried to understand the biological roles of arginylation in cardiovascular-associated proteins including β-actin (Asp3 arginylation) regulating cytoskeleton and cell motility[7,8], calreticulin (CALR, Asp18 arginylation) regulating stress granules in a Ca^{2+}-dependent manner[9,10], and RGS4/5/16 (tri-oxidized Cys2 arginylation) acting as nitric oxide and oxygen sensors[11,12]. Many of these studies focused on the implications of shortened half-lives of arginylated proteins involved in cardiovascular biology[1,7-12].

Meanwhile, many studies suggested that arginylation is also important for certain proteins to function properly (noncanonical roles) beyond its canonical role in the *N*-degron pathway[13,14]. It is reported that arginylation of β-amyloid guides proper α-helical shape preventing misfolding and aggregation[15]. Arginylation of α-synuclein (α-syn) facilitates brain health by preventing neurodegeneration[16,17]. Arginylation of calreticulin promotes its association with stress granules[18,19]. Decreased arginylation of nuclear proteins results in smaller nucleus size and architecture[20]. In addition, arginylation has been detected on histone proteins[20,21], potentially facilitating their interaction with DNA through the positively charged Arg residue installed post-translationally. Other prominent arginylated examples are chaperone HSPA5[22], BRCA1[23], PDI[24], and CDC6[25]. It is becoming clear that protein arginylation has many biological functions yet to be determined in regulating physiological processes. However, only a handful of proteins have been validated for their arginylation sites so far, and the discovery of arginylation substrates and their modification sites is becoming a bottleneck for the study of arginylation biology.

Identification of arginylation has been inherently challenging because both ATE1 and ribosome use the same arginine (Arg or R) source, arginyl-tRNA, to add an arginyl group to a protein, yielding posttranslational and translational addition respectively of arginyl with the same mass shift (+156 Da)[13] (**Fig. 1a**). This makes unbiased differentiation of posttranslational arginylation and translational arginine residues extremely difficult when both ATE1 and the ribosome are active (i.e., when cells are alive). In addition, arginylated proteins may go through the Arg/N-degron pathway for rapid ubiquitin-mediated degradation, decreasing the endogenous arginylation level for detection[13,25]. Furthermore, arginylation mostly happens on the protein *N*-termini after proteolytic cleavage, which is poorly understood for individual proteins in the whole proteome[13]. Additional confusion comes from trypsin miscleavage resulting in peptides starting with an R residue in bottom-up proteomics. Disregarding those challenges, efforts have been made aiming to systematically identify arginylation.

One early approach to screening arginylation substrates involved adding sub-divisions of a complete cDNA library to a transcription-translation-degradation system, which assumes that arginylated substrate is prone to the N-degron pathway[26]. A few arginylation substrates (*e.g.*, BiP and PDI) have been identified from the whole proteome through the combination of ATE1 assay *ex vivo* and [^{3}H]arginine autoradiography[24]. The autoradiography was also used for further identification of individual proteins (*e.g.*, CALR[10] and α-syn[16]) as ATE1 substrates. Notably, these methods heavily relied on mass spectrometry to reveal the arginylation sites on the labeled (*ex vivo*) proteins. In contrast, proteomic profiling was attempted to identify the endogenous (*in vivo*) arginylation sites from animal tissues using anti-arginylation antibody enrichment and proteomics. Such an approach enabled the first proteomics-based analysis to identify 43 plausible arginylated proteins[21]. Similarly, two later studies identified 19 and 15 proteins potentially modified by arginylation on their side-chain Asp and Glu residues[27,28], a different ATE1 catalysis mechanism from canonical *N*-term arginylation. However, most of those sites have little overlap with existing confirmed proteins/sites from *ex vivo* experiments and were largely postulated from search

algorithms without additional validation. Therefore, there is still a huge unmet need for the creation of an unbiased profiling method for the arginylation field at this stage.

Inspired by unbiased labeling using isotopic Arg[24] and the screening power of mass spectrometry-based proteomics[21], here we present a profiling technology for the unbiased discovery of ATE1 substrates and arginylation sites from complex whole proteomes (**Fig. 1b**). We first established the workflow using peptide and proteome-wide peptides as a proof-of-concept, then applied the technology to protein and whole proteomes for arginylation discovery. As a result, a large catalog of unbiased arginylation sites has been established from various cell and tissue samples. To facilitate data processing, a new computational tool, "ArginylomePlot", was developed and made publicly available for isotopic pair analysis. To be beneficial to the arginylation field and broader research community, we have established a publicly available database indexing all arginylation sites discovered from this study, allowing others interested in protein arginylation to have easy access to this growing type of data. This work could serve as the technological foundation for studying the functions of this essential PTM, and it will have a long-lasting impact on the arginylation field by opening new biochemical and biological frontiers.

Results

Isotopic arginylation of substrate peptide by ATE1 *in vitro*. To test the proof-of-concept of the designed activity-based arginylation profiling strategy (**Fig. 1b**), we started by isotopically labeling a standard peptide (modified from human β-actin sequence) with an open Asp (D) residue at the *N*-terminal. After LC-MS analysis, the extracted ion chromatograms of the differentially labeled products were manually examined for isotopic ratio (0.997) and co-elution of peaks (**Fig. 1c**). The data was also searched by Byonic to confirm the product identities (**Fig. S1**) whose MS1 spectra were extracted to validate the Arg^{10}/Arg^{0} pair features (doublets) and summarized into a boxplot for ratio/intensity overviews (**Fig. 1d**). The peptide labeling was replicated 4 times and produced consistent ratio profiles (**Fig. 1e**). An increasingly stringent MS1 pair detection using quartet ("2+2" peaks) and sextet ("3+3" peaks) yielded closer H/L ratios to hypothetical 1.0 than doublet ("1+1" peaks) but gave decreased numbers of MS1 pairs in all replicates. To ensure all MS1 pairs are included, we decided to use MS1 doublet as the threshold filter and include duodecet ("6+6" peaks) for pair overview as shown in **Fig. 1d**. In addition, different ratios can be used at H/L ratio = 0.5 or 0.7 (**Fig. S2-3**) if further ratio manipulation is needed. A H/L ratio of 1.0 is used in this study.

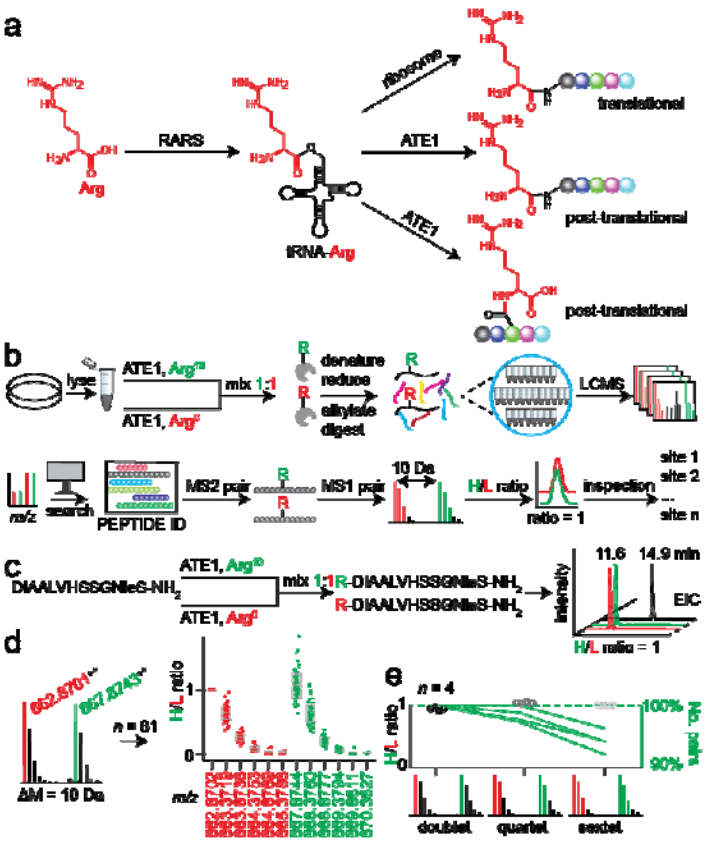

Figure 1. Isotopic arginine labeling and detection strategy for ATE1 substrates and arginylation sites. a, scheme of arginyl installation onto proteins by ribosomal synthesis (translational) and ATE1 (post-translational). RARS, arginine-tRNA ligase. ATE1, arginyl-tRNA-protein transferase 1. **b,** activity-based arginylation profiling platform for arginylation discovery from biological samples. Lysate is labeled by isotopic arginine molecules (Arg^{10} and Arg^{0}) respectively using ATE1 assay, mixed, and digested. Peptides are fractionated and analyzed by mass spec. Proteomics data is searched for all peptide IDs where MS2 pairs modified by heavy and light Arg are selected for their MS1 heavy/light feature and ratio inspection. **c**, isotopic arginylation of a peptide ATE1 substrate. **d**, isotopic feature in MS1 spectra and their summary. **e**, ratio summary of MS1 pairs in 4 replicates (n = 4) using doublet, quartet, and sextet peaks. The numbers of pairs in quartet and sextet are normalized to the numbers of pairs in doublet from respective replicate. EIC: extracted ion chromatogram. Nle: norleucine.

Development of in-house software for dataset analysis. Encouraged by the proof-of-concept data, we then aimed to develop a computational tool "ArginylomePlot" (**Fig. 2a**) with several capabilities to facilitate handling datasets from future complex samples. The software should be able to 1) filter out MS2 pairs with the same sequence modified by Arg^{10} and Arg^{0} (Δmass = 10.008269 Da) disregarding other modifications (*e.g.*, Met oxidation and Cys carbamidomethylation), 2) extract their MS1 scans from raw data, 3) summarize heavy/light ratios of each arginylation peptide, and 4) export paired MS1 and MS2 scans for data visualization and indexing. The software is publicly available to download on GitHub (https://github.com/BeckyHan/Garcia-Lab/tree/main/ArginylomePlot). Briefly, mzXML data converted from raw data was used as the source input data, and search results from proteomics software (*e.g.*, Byonic) were used as peptide input. Once a co-elution MS2 pair was identified from the peptide list, their MS1 information (*e.g.*, *m/z* and charge) was used to extract pairs from mzXML for ratio calculation. To present high-confidence proteomics data, peptide score (H or L ≥ 300) was applied as a filter before MS2 spectrum export. In the end, the software also exports spectra as Excel files for establishing a website database. An exemplary dataset and detailed instructions to execute the software are provided (**Supplementary Dataset 1**).

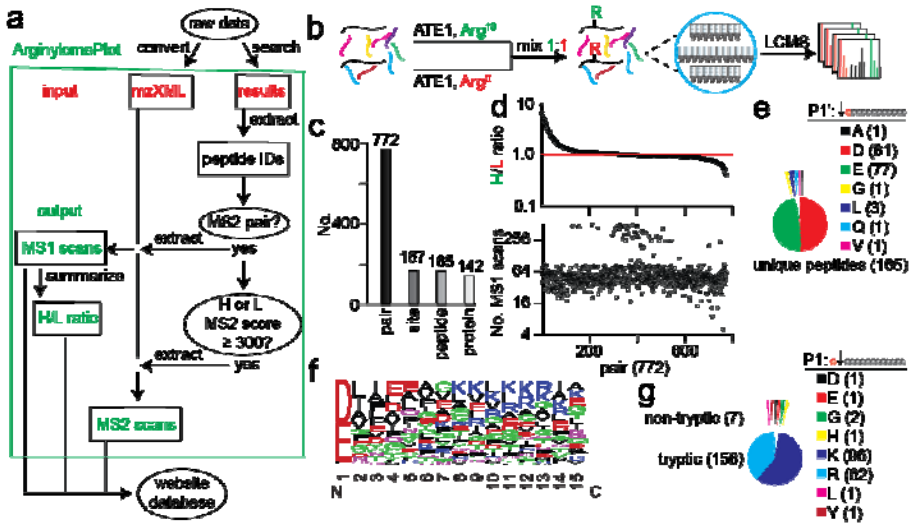

Figure 2. Arginylation analysis of whole-proteome peptides using in-house software. a, software flowchart of customized "ArginylomePlot". Input data are mzXML and peptide identification files. Output data are MS1, MS2, and the summary of unbiased arginylation sites. **b,** experimental workflow for arginylation of tryptic peptides from HEK293T (ATE1 KO) cells. **c,** numbers of identified MS1 pairs, arginylation sites, unique peptides, and unique proteins. **d,** H/L ratio distribution of all MS1 pairs and their corresponding numbers of MS1 scans. **e,** analysis of the *N*-terminal residues of all unique arginylated peptides. Q is arginylated after deamidation (Q→E). **f,** sequence logo calculated from unmodified forms of all unique arginylated peptides. Frequency plot is generated by WebLogo. **g,** comparison of tryptic and non-tryptic *N*-term of all arginylated peptides.

Isotopic arginylation of HEK293T peptides by ATE1 *in vitro*. Assisted by the software, we next tested the arginylation of a whole-proteome peptide mixture prepared from the whole proteome of HEK293T cells with ATE1 knocked out to avoid potential interference from endogenous arginylation (**Fig. 2b**). After data analysis, a total of 772 arginylation pairs belonging to 167 unique arginylation sites were detected at the MS1 level by the software (**Fig. 2c**, **Fig. S4**, **Table S1** and **Supplementary Dataset 2**). The data showed exclusive N-terminal arginylation using a peptide mixture (**Supplementary Dataset 2**), even though we searched for N-terminal and sidechain arginylation equally at the same time. Most of the peptide pairs (98.3%) are detected at charge states 2 and 3, with a small portion in charge 4 (**Fig. S5**). The distribution profile of H/L ratios (threshold: 0.1 ≤ ratio ≤ 10) from all MS1 pairs is centered at 1.0 (**Fig. 2d**) which is the ideal ratio for each labeled peptide per experimental design, demonstrating the success of the workflow for complex peptide sample. The doublet ratios were also compared with the quartet and sextet profiles (**Fig. S6**). The numbers of MS1 scans with the doublet feature used for generating respective H/L ratios are provided (**Fig. 2d**, **Fig. S7**). When looking at the arginylated *N*-term residues of all unique peptides, a majority of arginylation happened on D and E (including Q→E) residues (159 out of 165, 96.36%) (**Fig. 2e**) while the data also suggested possible arginylation on other *N*-term residues (*e.g.*, A, G, L and V), consistent with reported specificities and activities of ATE1[29,30]. We then generated the sequence logo of unique peptides using WebLogo 3.0[31]. The result suggested that arginylation favors *N*-term D and E residues significantly, while subsequent nonpolar residues (I, L, F, V and A) and acidic residues (D and E) may facilitate the peptide *N*-term arginylation (**Fig. 2f**). While most of the unique peptides (158 out of 165, 95.76%) are tryptic after K or R cleavage, a few non-tryptic peptides were arginylated (**Fig. 2g**). For example, the arginylation of SSBP E17 was on a non-tryptic peptide (**Fig. S8**), this may have resulted from endogenous protein *N*-term processing and cleavage[32]. This observation demonstrates the potential application of our peptide workflow for the discovery of the cleavage and arginylation of endogenous protein *N*-term.

Isotopic arginylation of protein substrates by ATE1 *in vitro*. We then moved forward from peptide to protein arginylation using CALR since it is known for *N*-term arginylation at the E18 site after endogenous cleavage of a signaling peptide (AA 1-17)[18]. Purified 18E-CALR after the cellular overexpression was isotopically labeled and yielded the H/L ratio of 1.0 in the arginylated E18 peptide

(R^{10}/R^{0}-E_{18}PAVYFK) (**Fig. 3a** and **Fig. S9**). The arginylation efficiency is calculated to be 64.7% for the E18 site based on MS2 spectrum counts of modified (R^{10}/R^{0}-EPAVYFK, counts = 33) and unmodified (EPAVYFK, counts = 18) peptides. Replication of CALR arginylation (n = 5) showed consistent ratios near 1.0 (**Fig. 3a** and **Fig. S10**). In addition, arginylation results (n = 5) of a commercial 18E-CALR (Abcam, ab276554) showed consistent E18 labeling (**Fig. S11**). In comparison, 18R-CALR protein was purified and tested, and the results (n = 5) showed nearly no R^{10} arginylation due to the absence of an open *N*-term E18 residue (**Fig. S12**).

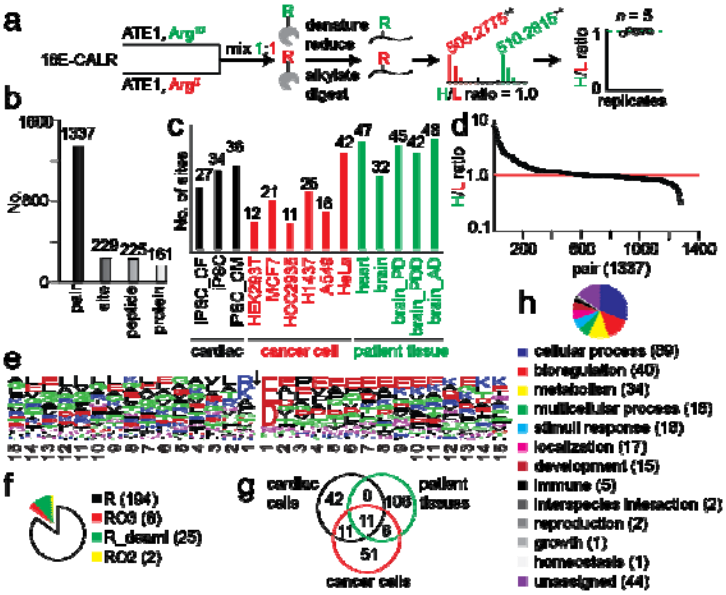

Figure 3. Summary of arginylation sites and ATE1 substrates in human proteins and proteomes. a, experimental workflow for CALR arginylation. **b,** numbers of identified MS1 pairs, arginylation sites, unique peptides and unique proteins in human cells and patient tissues. **c**, overview of arginylation sites in human cells and patient tissues. **d**, ratio plot of all MS1 pairs detected in all sample fractions. **e**, sequence logo calculated from unmodified forms of all unique arginylated peptides. Frequency plots are generated by WebLogo. **f**, arginylation type comparison of all unique sites. **g**, arginylation site comparison between sample types. **h**, biofunction analysis of ATE1 protein substrates using PANTHER. iPSC, induced pluripotent stem cell. CF, cardiac fibroblasts. CM, cardiomyocytes. R, arginylation. RO3, Cys tri-oxidation and arginylation. RO2, Cys di-oxidation and arginylation. R_deami, N/Q arginylation after deamidation. PD, Parkinson's disease. PDD, PD with dementia. AD, Alzheimer's disease.

Table 1. Number of detections/pairs for each arginylation site from human proteomes.

*CALR E18 R	100	CH60 Q42 R_deami	5	PLEC E4050 R	3	ACTC E109 R	1	MTDC E36 R	1
*PDIA1 D18 R	92	G3P D296 R	5	RLA1 D18 R	3	AKA12 E418 R	1	MYH6 E73 R	1
MBP D168 R	68	LN28A E18 R	5	TBA1B D327 R	3	AKAP2 D638 R	1	MYH7 D1008 R	1
*SSBP E17 R	67	MBP T200 R	5	AAK1 Q374 R_deami	2	AQP4 E279 R	1	MYH7 E1376 R	1
*RM12 C45 RO3	55	MYL3 E131 R	5	ACTB E107 R	2	AT5G1 D62 R	1	MYH7 E1489 R	1
A1AT E25 R	44	NFL E453 R	5	ACTB E241 R	2	ATAD5 V1449 R	1	MYH7 E927 R	1
NFL D468 R	38	NFM E497 R	5	ACTC C259 RO2	2	ATIF1 D28 R	1	MYH9 D1846 R	1
SAP D405 R	35	SAP G407 R	5	AKA12 E952 R	2	ATIF1 E42 R	1	MYOZ2 D255 R	1
CATD E64 R	33	SPTN1 E1124 R	5	ANK2 E1760 R	2	ATP5H D129 R	1	MYPT2 D816 R	1
CATD G65 R	28	TNNI3 E165 R	5	BACH C36 RO3	2	ATP5J N33 R_deami	1	NCAM1 E833 R	1
TBB5 E 3 R	25	TXND5 E40 R	5	CNBP Q44 R_deami	2	ATS15 D749 R	1	NDKM K91 R	1
*ERO1A E24 R	23	VIME E425 R	5	CWC15 Q45 R_deami	2	BI1 I 8R_deami	1	NECP1 C162 RO3	1
F162A C41 RO3	22	ACTC E318 R	4	EFHD2 Q67 R_deami	2	CALX E275 R	1	NEUG C 9RO3	1
ODO2 D68 R	21	ATIF1 E65 R	4	FCN1 D120 R	2	CC148 I574 R	1	NFL E509 R	1
MBP G277 R	18	CASQ2 E20 R	4	*GATB E42 R	2	CDY1 D285 R	1	NFM E884 R	1
MBP D216 R	17	CH60 D49 R	4	HBA D65 R_deami	2	CH60 C447 R	1	NOP16 E77 R	1
MBP E217 R	17	NFH E469 R	4	HS90B E539 R	2	CH60 D100 R	1	NPC2 E20 R	1
PGCB D23 R	16	NFL E507 R	4	HSP7C G372 R	2	CH60 D209 R	1	NUCL E628 R	1
*CH60 E107 R	15	NFM E599 R	4	LDB3 E257 R	2	CH60 G43 R	1	PCDH1 D944 R	1
MYH9 D1136 R	15	NHRF1 E121 R	4	LETM1 D116 R	2	COX17 D 6 R	1	PDLI5 E215 R	1
H4 D25 R	14	PGRC1 D49 R	4	MAP1A E663 R	2	COX41 D43 R	1	PDLI5 E297 R	1
MLRV E22 R	14	RD23B E136 R	4	MESD E35 R	2	DJC10 D33 R	1	PSD12 G331 R	1
GFAP E391 R	13	SCG1 D88 R	4	MLRV N154 R_deami	2	DPEP3 D150 R	1	PSMD6 L84 R	1
NFM E454 R	13	TBA1B D69 R	4	MYH7 E73 R	2	DREB D636 R	1	PTBP1 G306 R	1
NFM E470 R	12	AP180 N767 R_deami	3	NFL E469 R	2	DZI1L Q132 R	1	PTGDS E25 R	1
CLUS D23 R	10	APOA1 D25 R	3	NFM E763 R	2	E2F7 D10 R	1	RL23A E 8 R	1
GFAP D417 R	10	C99L2 D26 R	3	NPM D178 R	2	F205A E1023 R	1	RLA1 D19 R	1

NEUM E89 R	10	CALD1 E161 R	3	NPM D179 R	2	FUBP1 N369 R_deami	1	RM12 C45 R	1
NFM E496 R	10	CALU D62 R	3	NPM D180 R	2	GLYM Q27 R_deami	1	ROA1 E93 R	1
PDIA4 E25 R	10	CAVN2 Q161 R_deami	3	PACN1 N330 R_deami	2	HBA D48 R	1	RON D1232 R	1
DREB D634 R	9	CD99 D23 R	3	PGCB E26 R	2	HMGA1 E47 R	1	RS27 D 6 R	1
MBP N226 R_deami	9	G3P D315 R	3	PGCB E412 R	2	HMSD Q43 R_deami	1	RS7 E188 R	1
MYH7 E1821 R	9	H15 E 8 R	3	PTBP1 D 7 R	2	HNRPK D279 R	1	RT18A E37 R	1
ENPL D22 R	8	HACD3 P100 R	3	ROA2 D161 R	2	HNRPK Q358 R_deami	1	SCN1A V1579 RO2	1
NCAN E23 R	8	HNRPC D123 R	3	S10AE C74 RO3	2	HNRPL D284 R	1	SFPQ E696 R	1
RLA1 N62 R_deami	8	HNRPK N306 R	3	SCMC1 Q16 R_deami	2	HOOK1 D659 R	1	SNX17 E463 R	1
TAU N644 R_deami	8	HNRPU E259 R	3	TBB4A D67 R	2	IF4H D196 R	1	SPTB2 E1469 R	1
ACTC D53 R	7	KTN1 D238 R	3	TCAF1 V114 R	2	ILF2 D347 R	1	SRRT D866 R	1
BCLF1 E463 R	7	LDB3 N197 R_deami	3	TFF1 E25 R	2	JTB E31 R	1	SRRT D868 R	1
ACTB D51 R	6	MBP N226 R	3	TMM11 D163 R	2	KAD4 G82 R	1	TBA1B D251 R	1
CBS E 4 R	6	MYH7 D1229 R	3	UTP18 E374 R	2	KS6A1 D37 R	1	TBA4A D69 R	1
LMAN2 D45 R	6	MYH7 E1902 R	3	VIME D90 R	2	MAP1A E1580 R	1	TNNT2 D108 R	1
MCFD2 E27 R	6	NFL Q75 R_deami	3	XRCC5 E583 R	2	MAP1B Q907 R_deami	1	TYB4 D 6 R	1
MTAP2 Q431 R_deami	6	NFM E455 R	3	ACLY E830 R	1	MBP D279 R	1	VATD E242 R	1
MYH7 E1461 R	6	NT5D3 C44 RO3	3	ACTA E109 R	1	MITOK C37 RO3	1	VIME D451 R	1
SRCA E21 R	6	PELP1 E1008 R	3	ACTA E318 R	1	MPPB Q46 R_deami	1		

R, arginylation. RO3, Cys tri-oxidation and arginylation. RO2, Cys di-oxidation and arginylation. R_deami, N/Q arginylation after deamidation. *, validated by standard peptides.

Arginylation profiling in human proteomes. Using this established platform, we profiled 14 human samples after cell/tissue lysis and ATE1 assay *ex vivo*, a key to installing isotopic Arg post-translationally under ribosome-free conditions to bypass translational Arg incorporation and bias. A total of 1337 isotopically labeled pairs belonging to 229 unique arginylation sites on 161 proteins were identified (**Fig. 3b**, **Table 1**, **Supplementary Dataset 3**, and **Fig. S13-14**). Only 3 arginylation sites (S10AE C74 RO3, ACTC C259 RO2, and HMSD Q43 R_deami) were assigned as sidechain arginylation, accounting for 1.3% of all unique sites. Similar to results from HEK293T peptides, most of the peptide pairs are detected at charge states 2 (42.8%) and 3 (52.2%), with small portions in charges 4 (4.8%) and 5 (0.2%) (**Fig. S15**). As cross-validation, CALR E18 and PDIA D18 are the top-2 high-frequency sites with 100 and 92 detections (MS1 pairs) respectively, consistent with the literature on their confirmed E18[10] and D18[24] arginylation. The number of unique arginylation sites from each sample is listed in **Fig. 3c** which shows an average of 31 sites/sample could be identified. The biological samples cover induced pluripotent stem cells (iPSC), cardiac cells derived from the iPSC, commonly cultured cell lines, and clinical patient tissues, demonstrating the potential applicability of this method to a wide range of other human proteomes. The H/L ratios (threshold: 0.1 ≤ ratio ≤ 10) of MS1 pairs are distributed symmetrically and perfectly centered at the ideal ratio of **1.0** (**Fig. 3d**). The doublet ratios were also compared with the quartet and sextet profiles (**Fig. S16**). The numbers of MS1 scans with the doublet, quartet, and sextet features for generating respective H/L ratios are provided, quartet and sextet pairs showed lower numbers of qualified MS1 scans than doublets based on their trendlines (**Fig. S17**). The sequence logo from all unique peptides suggested that arginylation favors *N*-term D and E residues significantly, while subsequent nonpolar residues (A, L, V, and P) and acidic residues (D and E) may facilitate the peptide *N*-term arginylation (**Fig. 3e**). Interestingly, all theoretical types of arginylation have been detected including arginylation (R, 84.7%), Cys tri-oxidation arginylation (RO3, 3.5%), N/Q deamidation arginylation (R_deami, 10.9%), and Cys di-oxidation arginylation (RO2, 0.9%), (**Fig. 3f** and **Fig. S18**). Comparison of arginylation sites between iPSC, cancer, and patient samples showed only 30 (11+11+8) shared sites, while the remaining majority of sites are unique to their respective cell/sample groups (**Fig. 3g**). Comparisons between individual samples are listed in **Fig. S19** (cardiac), **Fig. S20** (brains), and **Fig. S21** (cancers), indicating unique and shared arginylation sites from individual samples. Among 161 proteins identified, 158 protein targets are involved in many key biological processes (*e.g.*, cellular process, biological regulation, and cellular metabolism) according to the PANTHER classification (**Fig. 3h**).

Validation of representative arginylation sites. We aimed to validate representative sites using synthetic peptides whose MS behaviors (MS1 spectra in **Fig. 4a** and MS2 spectra in **Fig. S22**) matched those in our MS data. The chosen sites are a mixture of known (CALR and PDIA) and unknown, and they represent high-frequency (CALR, PDIA, SSBP, and RM12), mid-frequency (ERO1A and CH60), and low-frequency (GATB) sites in our data from biological samples (**Table 1**). Such a validation added extra confidence to the Arg10 arginylation which is an unnatural process and thus can be considered an internal validation of our workflow. For example, H/L ratio = 1.0 for RM12 C45 arginylation (**Fig. 4b**) eliminated the possibility of tryptic missed cleavage between Arg44 and tri-oxidized Cys45, standard peptide confirmed this minor type of arginylation with co-presence of Cys trioxidation[1] (**Fig. S22**). It is noteworthy that the low frequency of a site doesn't necessarily mean low confidence since most of the

reported sites are based on many isotopic co-eluting MS1 scans (**Fig. S17** and **Supplementary Dataset 3**) and paired MS2 spectra (**Supplementary Dataset 4**).

We then selected two novel sites for validating their arginylation in an ATE1-protein co-expression system in *E. coli*[33]: a chaperone ERO1A in the endoplasmic reticulum (ER), being similar to CALR and PDIA; and SSBP being distinct from ER proteins in molecular size (17 kDa), localization (mitochondria) and function (single-stranded DNA-binding). The results showed that both ERO1A E24 and SSBP 17E were arginylated (**Fig. 4c** and **Fig. S23-24**). As a bonus, we also detected a further leucylation on top of arginylation (**Fig. S23-24**), a unique process to modify *N*-term Arg due to the presence of the *E. coli* leucyl/phenylalanyl-tRNA-protein transferase (LFTR)[34]. We also tested the peptide-ubiquitin conjugates of ERO1A and SSBP with open *N*-term E24 and 17E, which were also arginylated in the co-expression system (**Fig. S25**). The arginylation and leucylation were also observed by top-down proteomics (**Fig. S26-27**). The results concluded that ERO1A E24 and SSBP 17E are arginylation target sites of ATE1.

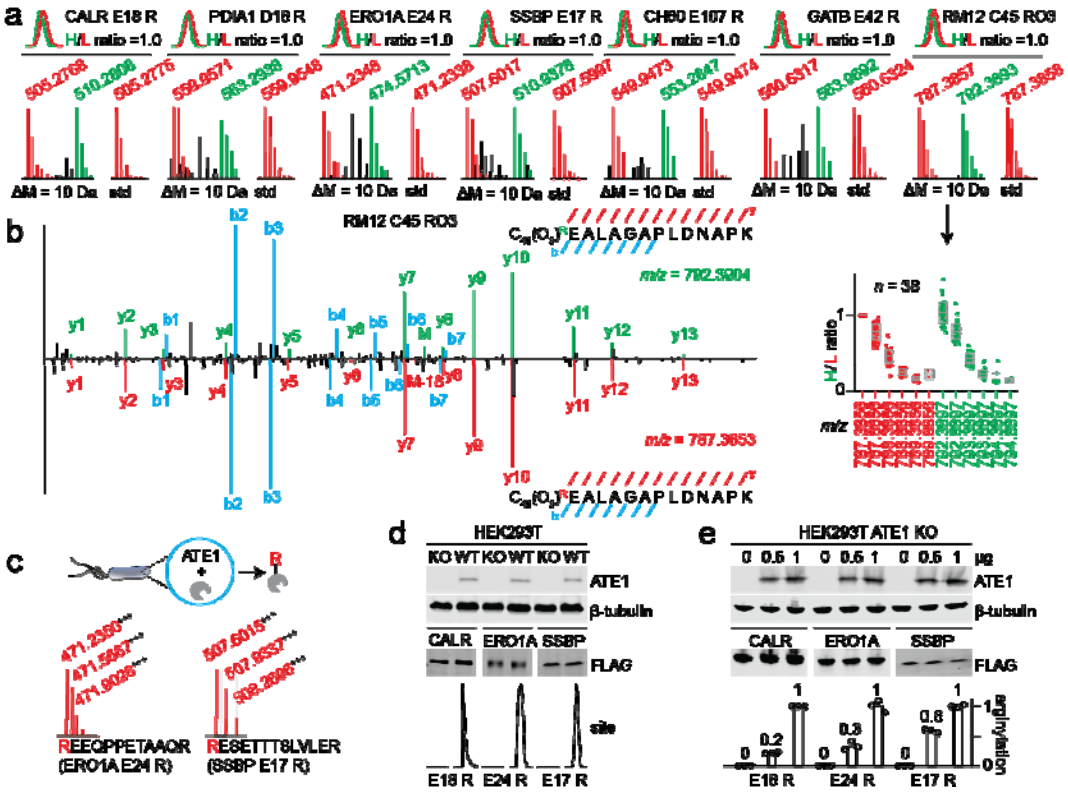

Figure 4. Validation of representative arginylation sites. a, synthetic peptide validation of 7 arginylation sites. **b,** representative MS2 spectra indicating RM12 arginylation on Cys45 with tri-oxidation (C45 RO3). **c,** open E24 in ERO1A and E17 in SSBP are arginylated in ATE1-protein co-expression system. **d,** arginylation dependency on endogenously expressed ATE1. **e,** arginylation correlation to ATE1 overexpression levels. std, standard peptide. KO, ATE1 KO. R, arginylation.

The unbiased nature of the profiling method is owing to the co-elution strategy of isotopic Arg10/Arg0 peptides, however, the revealed sites are based on an *ex vivo* ATE1 assay and thus do not necessarily conclude their occurrences *in vivo* (in cells) where ATE1 is active. To confirm endogenous arginylation activity on the identified targets in cells, we overexpressed the wild-type ERO1A and SSBP in HEK293T cells using CALR as a positive control. The results show that all three sites (CALR E18, ERO1A E24 and SSBP 17E) are arginylated after purification and proteomics analysis (**Fig. 4d** and **Fig. S28**). As a comparison, we also performed the same experiment in HEK293T (ATE1 KO) cells, which did not show any arginylation on those sites indicating their dependency on ATE1. To further test their dose-dependency on ATE1, we then co-overexpressed the ATE1 and protein substrates in HEK293T (ATE1 KO) cells. The data show the arginylation levels of the tested sites are dose-dependent on the ATE1 expression (**Fig. 4e**). Such dose-dependency was also observed when co-overexpressing CALR and

ATE1 in WT HEK293T cells (**Fig. S29**). Both ERO1A[35] and SSBP[36] contain cleavage peptides before the arginylation sites (E24 and 17E respectively), similar to that of CALR. Taking advantage of this feature, we further prepared 24R-ERO1A and 17R-SSBP plasmids by inserting an R residue before E, their arginylated peptides (**Fig. S30**) resulted from overexpression, affinity purification and proteomics further confirmed the arginylation of their wild-type counterparts.

We have additionally validated the endogenous arginylation of two more sites (proteins): A1AT E25 arginylation (**Fig. S31**) and Tau N644 arginylation after deamidation (**Fig. S32**). Similar to CALR, ERO1A and SSBP, A1AT has a signal peptide[37] before E25 thus it is not surprising to observe its E25 arginylation by endogenous ATE1. Tau N644 has been arginylated after deamidation in our data, which has never been observed previously. We also confirmed the arginylation of this site using overexpression (**Fig. S32**). We have additionally confirmed the arginylation of the Tau E3 site (**Fig. S32**), which was proposed previously as a substrate of ATE1, but not validated for its arginylation[38]. A previous study showed that purified Tau did not show detectable arginylation by ATE1 *in vitro*[16], possibly due to the lack of exposed arginylation sites (*e.g.*, E3 and N644 deamidation). Different from Tau E3 as a calpains cleavage product[38], the mechanism of generating an open N644 followed by deamidation for arginylation remains to be elucidated.

Biological functions associated with ERO1A arginylation. To investigate whether arginylated ERO1A resides in ER, we did imaging on overexpressed ERO1A and 24R-ERO1A. Both proteins co-localized with ER marker and PDI (**Fig. 5a** and **Fig. S33**), suggesting that 24R-ERO1A was translocated into ER after signaling peptide AA1-23 cleavage. As a positive control, we showed that CALR-halo and its arginylation form co-localized with a GFP-tagged ER marker (**Fig. S34**). Similar to CALR and PDIA, ERO1A is translocated into ER after signal peptide cleavage. A previous study reported the formation of the ERO1A-PDI complex in regulating cellular function[39], our pulldown data showed that 24R-ERO1A interacted with PDI to a comparable extent with and without PDI co-overexpression (**Fig. S35-36**). We also showed that arginylation of ERO1A maintains its enzymatic activity on oxidative protein folding compared with WT ERO1A as indicated by the disappearance of the reduced JcM band (**Fig. S37a**). To investigate the arginylation effect on ERO1A stability and degradation, we compared the degradation patterns of cytosolic ERO1A fusion proteins with and without arginylation (**Fig. S37b**) according to similar experiments on CALR[40]. Levels of 24E-ERO1A and 24R-ERO1A are decreased after CHX treatment to inhibit protein synthesis compared to experiments without CHX (**Fig. S35b**), suggesting that they are both involved in cytosolic degradation. Treatment with higher concentrations of MG132 increased the ERO1A levels in different groups of experiments (**Fig. S35b**). To take a closer look at the differences between 24E-ERO1A and 24R-ERO1A proteins, we did CHX chase experiments and the results showed that 24R-ERO1A was less prone to degradation than 24E-ERO1A with clear degradation after CHX treatment (**Fig. 5b**). Such behavioral differences have been previously observed in cytosolic CALR[40], suggesting that arginylation of ERO1A may also have a stabilization effect against proteasomal degradation.

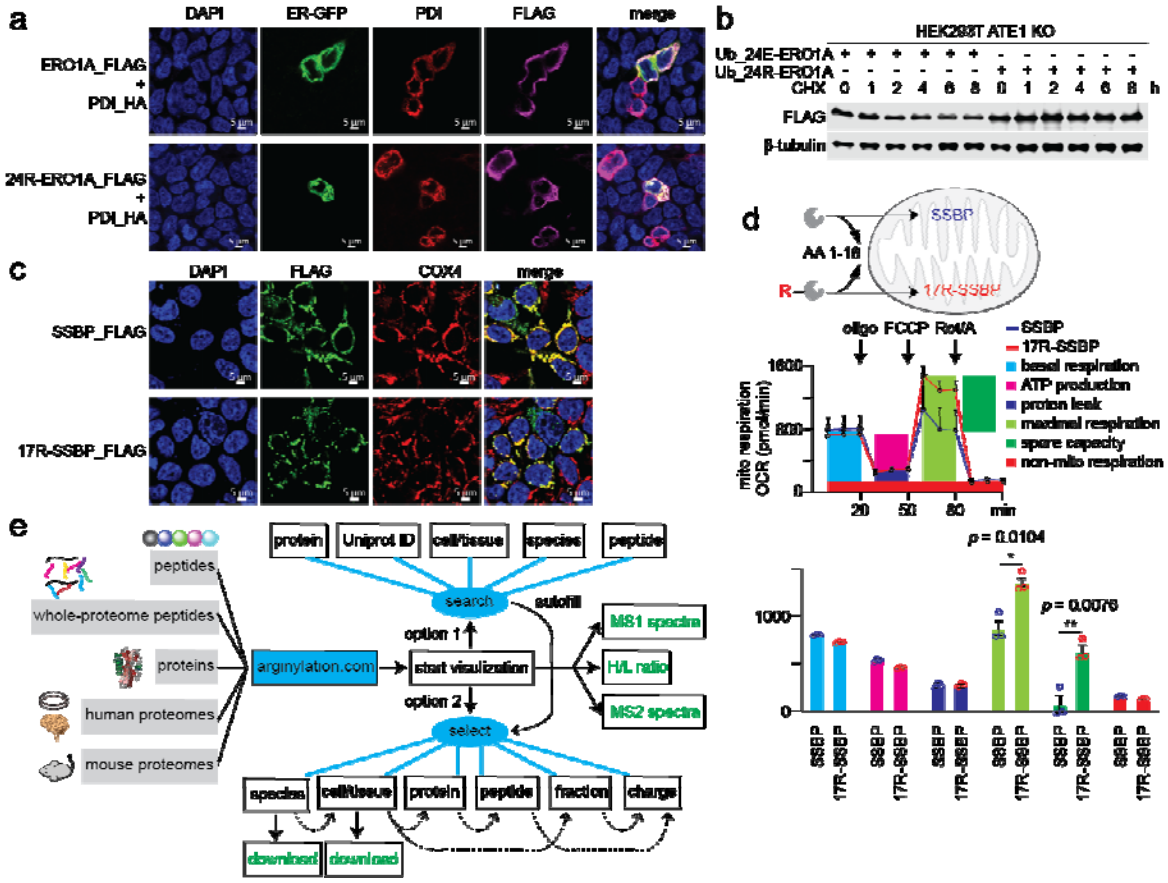

Figure 5. Biological functions of representative arginylation sites indexed by a public website. a, imaging of ERO1A and 24R-ERO1A compared with ER marker and co-overexpressed PDI. **b**, expression levels of cytosolic ERO1A species in CHX chase experiment. **c,** imaging of SSBP and 17R-SSBP compared with mitochondria protein COX4. **d**, bioenergetic profiles of HEK293T cells after SSBP and 17R-SSBP transfection measured by Seahorse XF24. Mitochondria respiration was analyzed with basal respiration, ATP production, proton leak, maximal respiration, spare capacity, and non-mitochondria respiration. The average values of 3 Seahorse measurements were used for comparison. 5 biological replicates (n = 5 wells) were used for each plasmid. A two-tail Student's t-test was used. $*p < 0.05$, $**p < 0.01$, $***p < 0.005$, $***p < 0.001$. **e,** Design and flowchart of the arginylation database and its website. Arginylation data are from peptides, whole-proteome peptides, proteins, human proteomes, and mouse proteomes. Visualization includes isotopic ratios and annotated isotopic MS1 and MS2 spectra. All indexed MS1 and MS2 scans are accessible to the public to download. A dashed arrow means a one-to-multiple inclusion relationship.

Biological functions associated with SSBP arginylation. SSBP matures by translocation into mitochondria after cleavage of its transit peptide (AA 1-16)[36]. We did imaging on SSBP and 17R-SSBP to investigate whether arginylated SSBP resides in the mitochondria. Both species co-localized with mitochondria protein COX4 (**Fig. 5c** and **Fig. S38**), suggesting that 17R-SSBP was translocated into mitochondria after cleavage of its transit peptide AA1-16. When checking cytosolic SSBP for the N-degron pathway using a ubiquitin cleavage plasmid system, we did not observe an obvious response toward MG132 treatment (proteasome inhibitor) (**Fig. S39**). CHX treatment (protein synthesis inhibitor) reduced the expression levels of both 17E-SSBP and 17R-SSBP compared with cells not treated with CHX, indicating cellular protein turnover of both species. 17R-SSBP expression levels were higher than WT SSBP with and without CHX treatment, indicating a slower turnover of 17R-SSBP than SSBP. The results suggest that the major role of SSBP arginylation might not be degradation (**Fig. S39**). We then turned our attention to mitochondrial SSBP. SSBP KO in mouse models is embryonic lethal whereas conditional KO in the heart results in cardiomyopathy and reduced life span (~18 weeks) accompanied by heart

respiratory chain deficiency[41]. It is noteworthy that ATE1 KO is also embryonic lethal with heart defects[1], being similar to SSBP KO. Thus arginylation of SSBP may regulate cells through mitochondria functions. Considering the importance of mitochondria in energy generation and heart functions, we then investigated the functional differences between SSBP and 17R-SSBP on cellular bioenergetics (**Fig. 5d**) based on a previous study on SSBP mutants[42]. Analysis of cellular oxygen consumption rate (OCR) showed that HEK293T cells overexpressing 17R-SSBP displayed comparable basal respiration, ATP production, and non-mitochondria respiration than WT SSBP (**Fig. 5d**). Interestingly, 17R-SSBP resulted in significantly higher maximal respiration (p = 0.0104) and spare capacity (p = 0.0076) than cells overexpressing WT SSBP (**Fig. 5d** and **Fig. S40** and **Supplementary Dataset 5**). The relative ratios of maximal respiration and spare capacity in 17R-SSBP are 1.6 and 8.5 compared with WT SSBP (**Fig. S40**), indicating improved mitochondria respiration potential after SSBP arginylation.

Arginylation profiling in mouse tissues. Our profiling platform has been working in human cells and tissues, to test its general applicability we next applied it to mouse tissues. We acknowledge that it is not ideal to use human ATE1 to arginylate mouse proteomes, although such a cross-species approach has been previously used[16]. Results from three tissues (lung, heart, and brain) showed that the platform is applicable to arginylation discovery from mouse proteome (**Supplementary Dataset 6**). A total of 14 sites from 69 MS1 pairs were identified (**Fig. S41**). Interestingly, CALR D18 and A1AT1 E25 are the two shared arginylation sites across three tissues. We noticed that the mouse A1AT1 E25 site was identified by a different peptide sequence (EDVQETDTSQK) (**Fig. S42**) from human A1AT E25 (EDPQGDAAQK) (**Fig. S31**). In addition, human and mouse E18 sites were also identified from species-dependent sequences (EPAVYFK and DPAIYFK, respectively) (**Fig. S43**), indicating that mouse and human sites can be used to cross-validate each other when overlapped.

Establishing a public database for arginylation sites and ATE1 substrates. We envision that the arginylation sites discovered from the various samples will greatly advance the arginylation and N-degron fields. The fact that our high-frequency hits (CALR, PDIA, and TAU *et al*)[25,38] are among the most intensively studied arginylation proteins instilled confidence to follow the biology of new sites. This represents a major advantage of our innovative method compared to existing profiling methods[21,28]. Meanwhile, we understand that we alone can't follow up on all the targets/sites for biological function, a publicly accessible database/website (www.arginylation.com, **Fig. 5e**) was thus formulated to allow everyone to examine our data and follow the biology of their arginylation targets of interest. The isotopic MS1 and MS2 scans discussed in this work from standard peptides, whole-proteome peptide mixtures, pure proteins, human proteomes, and mouse proteomes are included on the website. The source code for data visualization is publicly available to download at https://github.com/ChenfengZhao/Arginylation. The website was designed to allow the following two capabilities, 1) users can search protein names, accession numbers, sample types, species, and peptide sequences of their interest; 2) users can manually select species, sample types, proteins, peptides, fractions of a sample, and charge states of the peptides from our indexed database (**Fig. 5e**). As a result, all isotopic MS1 scans, H/L ratio summaries, and H/L MS2 scans with default settings are displayed on the website. To allow users to change our default parameters, we enabled changes in m/z errors and MS2 ion types. The most important feature of our website is that users can download our indexed data (MS1 and MS2 spectra in Excel format) based on species (*e.g.*, human and mouse) or samples (*e.g.*, iPSC or patient brain).

Discussion

ATE1 is the only enzyme known to catalyze arginylation in mammalian systems (*e.g.*, human and mouse), it has two isoforms in humans (ATE1-1 and ATE1-2) and four isoforms in mice (ATE1-1, ATE1-2, ATE1-3, ATE1-4). (**Fig. S44**)The expression levels and enzymatic functions vary among different isoforms[24,43]. While our work mostly focuses on establishing a general proteomic platform using human ATE1-1, using other isoforms (ATE1-2 for human proteomes, and mouse isoforms for mouse proteomes) for arginylation discovery is a necessary next step to cover the ATE1 substrate scope comprehensively. We preliminarily compared human ATE1-1 and ATE1-2 for arginylation profiling in two samples (patient brain and HeLa cells). ATE1-1 and ATE1-2 sites showed unique and shared sites, more arginylation sites were revealed by ATE1-1 than ATE1-2 for both samples (**Fig. S45-46**), indicating that ATE1-1 may have a slightly broader substrate scope for such an *ex vivo* arginylation assay. In addition, previous studies showed that the expression of ATE1 isoforms is tissue-specific and cell-dependent[24,43], thus the

expression levels might be a significant consideration when choosing ATE1 isoforms for arginylation profiling experiments.

It was initially believed that arginylation occurred only on exposed *N*-terminal Asp, Glu and Cys residues resulting in protein degradation by the ubiquitin-dependent *N*-degron pathway[44]. Later studies identified proteins (*e.g.*, α-synuclein[16]) potentially modified by arginylation on their sidechain Asp and Glu residues[27], resulting from a different but minor catalysis mechanism of ATE1. Our arginylation sites were identified using a search algorithm considering both *N*-term and sidechain arginylation situations (**Fig. S18**). The resulting sites from the whole-proteome peptide mixture (**Fig. 2**) and proteomes (**Fig. 3**) are in agreement with the current understanding that ATE1 predominantly arginylate protein/peptide *N*-term C (oxidized), D, and E residues, while other residues and sidechains can be arginylated less preferably. Since the ATE1 assay was performed on proteomes, we believe most sites were arginylated as protein *N*-term (**Fig. 3** and **Supplementary Dataset 3**). A preliminary analysis of the P1 residues (protease cleavage site) in arginylated peptides showed potential protease cleavage after each of the 20 amino acid residues (**Fig. S47** and **Supplementary Dataset 3**). While some sites (*e.g.*, CALR E18, ERO1A E24, and SSBP E18) were known to be protein *N*-term based on the current knowledge on cleavages of signaling peptides and transit peptides, many sites (*e.g.*, TAU N644) are left unexplained as to how the parent proteins were cleaved to expose the *N*-term sites for ATE1 arginylation. Previous studies have offered some insights into protease cleavage (*e.g.*, calpains for TAU E3[38] and caspase 3 for CDC6 D101[25]) for *N*-term arginylation, however, the cleavage products of more than 600 proteases remain elusive. Great efforts are needed to understand the interplay between proteolytic cleavage and arginylation.

Proteomic discovery of endogenously low-level arginylation from cells or tissues is challenging[21,28]. This is largely due to 1) the mass difference (+156 Da) introduced by arginylation being the same as the normal arginyl residue from a protein sequence, making label-free proteomics biased to predefined arginylation sites by nature; and 2) efficient enrichment (purification) methods are lacking. The fact that arginyl-tRNA is the same source of arginylation and ribosomal translation makes unbiased endogenous arginylation discovery almost impossible since one can't exclude ribosomal incorporation when cells are alive[13]. Our initial effort using Arg10 and Arg0 for pulse labeling of arginylation in HEK293T cells yielded a putative list of sites (**Fig. S48**). Additional efforts using cycloheximide to stop protein synthesis, MG132 to accumulate arginylation, and peptide fractionation to boost peptide IDs did not seem to increase our confidence. Arginylation identification from a standard proteome-wide peptide mixture is not ideal. Previous studies tried to use anti-arginylation antibodies to reduce sample complexity and enrich endogenous arginylation[21,28], however, these efforts by design were biased toward non-degradative ATE1 targets and hi-abundance proteins. Sites from those studies showed nearly no overlap with those previously characterized by the Varshavsky group as degradation-inducing arginylation substrates[13]. We thus turned our attention to an *ex vivo* ATE1 enzyme approach using cell lysates, which might be less physiologically relevant than those targeting endogenous arginylation. However, due to its unbiased nature, this method represents a superior strategy for arginylation discovery.

This profiling method relies on peptide fractionation to discover the low-abundance arginylated peptides, and intact peptides that are not of interest (accounting for >99.99%) are obvious interfering signals in proteomics data. The reduced signal complexity of each peptide fraction after fractionation is key to identifying arginylated pairs from proteome-wide samples. Without enrichment, the sites revealed by our method could be dependent on the expression levels of their parent proteins. We envisioned enrichment approaches are essential to achieve improved sensitivity and efficiency in arginylation site detection. Since ATE1 mainly installs Arg to *N*-term of substrates, some technologies targeting *N*-term peptides might be helpful for rginylation enrichment. Examples are TAILS (terminal amine isotopic labeling of substrates) technology[45] and iNrich (integrated *N*-terminal peptide enrichment) method[46] which are currently under our investigation as future directions. The anti-arginylation antibody enrichment is also under consideration; however, it may require scaling up the ATE1 reaction to milligram proteomes from the current 20-µg scale.

Methods

Methods section is provided in the Supplementary Information with details available.

Acknowledgments

B.A.G. thanks partial support from NIH NS111997, NIH HD106051, and NSF CHE 2127882 grants. Z.L. thanks a WUSM BMB Seed Grant (PJ000027587) and support from the Research Education Component through Grant Number P30 AG066444. D.L. thanks an NCI R21 grant (CA286307) and the support of the Mays Cancer Center Early Career Pilot Award from CCSG (P30 CA054174). Y.Z. thanks an NIH R35 GM150678 grant. M.J.G. thanks partial support from NIH (R01 HL141086), Children's Discovery Institute of Washington University and St. Louis Children's Hospital (PM-LI-2019-829), and the American Heart Association (970198). A. K. thanks the support from NIH R35GM122505 and R01NS102435. The authors thank Professor Natalie Niemi (WashU) for guidance on the Seahorse assay, Professor Xia Liu and Professor Guangyong Peng (WashU) for providing mouse tissues, and Washington University Diabetes Research Center supported by NIH Grant 5P30 DK020579.

Author contributions

Z.L. and B.A.G. conceived the project. Z.L., Y.X., and J.G. performed proof-of-concept experiments. Z.L., Y.X., J.G., X.Liu, E.Z., B.B.P., D.R., R.M.S., F.N.V., G.P.D., B.M., X.Lan, D.F., and L.G. performed experiments. Z.L., Y.X., J.G., X.Liu, E.Z., B.B.P., D.R., B.M., X.Lan, D.F., L.G., Y.Z., K.J.L., M.J.G., D.L., A.K. and B.A.G. analyzed data. Z.L. wrote the draft. C.Z. wrote Python codes and established the website, and X.H. wrote R codes and ArginylomePlot software. K.J.L., B.M., and A.K. provided patient tissues. All authors wrote, revised, and approved the manuscript.

Competing interests

Z.L., D.L., and B.A.G. are co-founders of LasNova Therapeutics, LLC.

Data availability

Arginylation site data are publicly available to view and download from www.arginylation.com (the website will be accessible during peer review and after publication, it will be inaccessible during revision).

Data supporting the findings in this study are available within the paper.

Any associated data are available from the corresponding authors upon request.

Code availability

Python codes for website construction are available to download from GitHub (link: https://github.com/ChenfengZhao/Arginylation)

R codes for ArginylomePlot software are available to download from GitHub (link: https://github.com/BeckyHan/Garcia-Lab/tree/main/ArginylomePlot).

The arginylation website is publicly accessible (link: www.arginylation.com) for data visualization and download.

References

1 Kwon, Y. T., Kashina, A. S., Davydov, I. V., Hu, R. G., An, J. Y., Seo, J. W., Du, F. & Varshavsky, A. An essential role of N-terminal arginylation in cardiovascular development. *Science* **297**, 96-99, (2002). PMID: 12098698

2 Lian, L., Suzuki, A., Hayes, V., Saha, S., Han, X., Xu, T., Yates, J. R., 3rd, Poncz, M., Kashina, A. & Abrams, C. S. Loss of ATE1-mediated arginylation leads to impaired platelet myosin phosphorylation, clot retraction, and in vivo thrombosis formation. *Haematologica* **99**, 554-560, (2014). PMID: 24293517

3 Kurosaka, S., Leu, N. A., Pavlov, I., Han, X., Ribeiro, P. A., Xu, T., Bunte, R., Saha, S., Wang, J., Cornachione, A., Mai, W., Yates, J. R., 3rd, Rassier, D. E. & Kashina, A. Arginylation regulates myofibrils to maintain heart function and prevent dilated cardiomyopathy. *J Mol Cell Cardiol* **53**, 333-341, (2012). PMID: 22626847

4 Singh, K., Gupta, A., Sarkar, A., Gupta, I., Rana, S., Sarkar, S. & Khan, S. Arginyltransferase knockdown attenuates cardiac hypertrophy and fibrosis through TAK1-JNK1/2 pathway. *Sci Rep* **10**, 598, (2020). PMID: 31953451

5 Kurosaka, S., Leu, N. A., Zhang, F., Bunte, R., Saha, S., Wang, J., Guo, C., He, W. & Kashina, A. Arginylation-dependent neural crest cell migration is essential for mouse development. *PLoS Genet* **6**, e1000878, (2010). PMID: 20300656

6 Leite, F. S., Minozzo, F. C., Kalganov, A., Cornachione, A. S., Cheng, Y. S., Leu, N. A., Han, X., Saripalli, C., Yates, J. R., 3rd, Granzier, H., Kashina, A. S. & Rassier, D. E. Reduced passive force in skeletal muscles lacking protein arginylation. *Am J Physiol Cell Physiol* **310**, C127-135, (2016). PMID: 26511365

7 Karakozova, M., Kozak, M., Wong, C. C., Bailey, A. O., Yates, J. R., Mogilner, A., Zebroski, H. & Kashina, A. Arginylation of beta-actin regulates actin cytoskeleton and cell motility. *Science* **313**, 192-196, (2006). PMID: 16794040

8 Zhang, F., Saha, S., Shabalina, S. A. & Kashina, A. Differential arginylation of actin isoforms is regulated by coding sequence-dependent degradation. *Science* **329**, 1534-1537, (2010). PMID: 20847274

9 Carpio, M. A., Lopez Sambrooks, C., Durand, E. S. & Hallak, M. E. The arginylation-dependent association of calreticulin with stress granules is regulated by calcium. *Biochem J* **429**, 63-72, (2010). PMID: 20423325

10 Decca, M. B., Carpio, M. A., Bosc, C., Galiano, M. R., Job, D., Andrieux, A. & Hallak, M. E. Post-translational arginylation of calreticulin: a new isospecies of calreticulin component of stress granules. *J Biol Chem* **282**, 8237-8245, (2007). PMID: 17197444

11 Hu, R. G., Sheng, J., Qi, X., Xu, Z., Takahashi, T. T. & Varshavsky, A. The N-end rule pathway as a nitric oxide sensor controlling the levels of multiple regulators. *Nature* **437**, 981-986, (2005). PMID: 16222293

12 Lee, M. J., Tasaki, T., Moroi, K., An, J. Y., Kimura, S., Davydov, I. V. & Kwon, Y. T. RGS4 and RGS5 are in vivo substrates of the N-end rule pathway. *Proc Natl Acad Sci U S A* **102**, 15030-15035, (2005). PMID: 16217033

13 Varshavsky, A. N-degron and C-degron pathways of protein degradation. *Proc Natl Acad Sci U S A* **116**, 358-366, (2019). PMID: 30622213

14 Kim, B. H., Kim, M. K., Oh, S. J., Nguyen, K. T., Kim, J. H., Varshavsky, A., Hwang, C. S. & Song, H. K. Crystal structure of the Ate1 arginyl-tRNA-protein transferase and arginylation of N-degron substrates. *Proc Natl Acad Sci U S A* **119**, e2209597119, (2022). PMID: 35878037

15 Bongiovanni, G., Fidelio, G. D., Barra, H. S. & Hallak, M. E. The post-translational incorporation of arginine into a beta-amyloid peptide increases the probability of alpha-helix formation. *Neuroreport* **7**, 326-328, (1995). PMID: 8742481

16 Wang, J., Han, X., Leu, N. A., Sterling, S., Kurosaka, S., Fina, M., Lee, V. M., Dong, D. W., Yates, J. R., 3rd & Kashina, A. Protein arginylation targets alpha synuclein, facilitates normal brain health, and prevents neurodegeneration. *Sci Rep* **7**, 11323, (2017). PMID: 28900170

17 Zhao, J., Pan, B., Fina, M., Huang, Y., Shimogawa, M., Luk, K. C., Rhoades, E., Petersson, E. J., Dong, D. W. & Kashina, A. alpha-Synuclein arginylation in the human brain. *Transl Neurodegener* **11**, 20, (2022). PMID: 35395956

18 Lopez Sambrooks, C., Carpio, M. A. & Hallak, M. E. Arginylated calreticulin at plasma membrane increases susceptibility of cells to apoptosis. *J Biol Chem* **287**, 22043-22054, (2012). PMID: 22577148

19 Carpio, M. A., Decca, M. B., Lopez Sambrooks, C., Durand, E. S., Montich, G. G. & Hallak, M. E. Calreticulin-dimerization induced by post-translational arginylation is critical for stress granules scaffolding. *Int J Biochem Cell Biol* **45**, 1223-1235, (2013). PMID: 23567256

20 Saha, S., Wong, C. C., Xu, T., Namgoong, S., Zebroski, H., Yates, J. R., 3rd & Kashina, A. Arginylation and methylation double up to regulate nuclear proteins and nuclear architecture in vivo. *Chem Biol* **18**, 1369-1378, (2011). PMID: 22118671

21 Wong, C. C., Xu, T., Rai, R., Bailey, A. O., Yates, J. R., 3rd, Wolf, Y. I., Zebroski, H. & Kashina, A. Global analysis of posttranslational protein arginylation. *PLoS Biol* **5**, e258, (2007). PMID: 17896865

22 Cha-Molstad, H., Sung, K. S., Hwang, J., Kim, K. A., Yu, J. E., Yoo, Y. D., Jang, J. M., Han, D. H., Molstad, M., Kim, J. G., Lee, Y. J., Zakrzewska, A., Kim, S. H., Kim, S. T., Kim, S. Y. *et al.* Amino-terminal arginylation targets endoplasmic reticulum chaperone BiP for autophagy through p62 binding. *Nat Cell Biol* **17**, 917-929, (2015). PMID: 26075355

23 Xu, Z., Payoe, R. & Fahlman, R. P. The C-terminal proteolytic fragment of the breast cancer susceptibility type 1 protein (BRCA1) is degraded by the N-end rule pathway. *J Biol Chem* **287**, 7495-7502, (2012). PMID: 22262859

24 Hu, R. G., Brower, C. S., Wang, H., Davydov, I. V., Sheng, J., Zhou, J., Kwon, Y. T. & Varshavsky, A. Arginyltransferase, its specificity, putative substrates, bidirectional promoter, and splicing-derived isoforms. *J Biol Chem* **281**, 32559-32573, (2006). PMID: 16943202

25 Yoo, Y. D., Mun, S. R., Ji, C. H., Sung, K. W., Kang, K. Y., Heo, A. J., Lee, S. H., An, J. Y., Hwang, J., Xie, X. Q., Ciechanover, A., Kim, B. Y. & Kwon, Y. T. N-terminal arginylation generates a bimodal degron that modulates autophagic proteolysis. *Proc Natl Acad Sci U S A* **115**, E2716-E2724, (2018). PMID: 29507222

26 Davydov, I. V. & Varshavsky, A. RGS4 is arginylated and degraded by the N-end rule pathway in vitro. *J Biol Chem* **275**, 22931-22941, (2000). PMID: 10783390

27 Wang, J., Han, X., Wong, C. C., Cheng, H., Aslanian, A., Xu, T., Leavis, P., Roder, H., Hedstrom, L., Yates, J. R., 3rd & Kashina, A. Arginyltransferase ATE1 catalyzes midchain arginylation of proteins at side chain carboxylates in vivo. *Chem Biol* **21**, 331-337, (2014). PMID: 24529990

28 MacTaggart, B., Shimogawa, M., Lougee, M., Tang, H. Y., Petersson, E. J. & Kashina, A. Global Analysis of Post-Translational Side-Chain Arginylation Using Pan-Arginylation Antibodies. *Mol Cell Proteomics* **22**, 100664, (2023). PMID: 37832787

29 Wadas, B., Piatkov, K. I., Brower, C. S. & Varshavsky, A. Analyzing N-terminal Arginylation through the Use of Peptide Arrays and Degradation Assays. *J Biol Chem* **291**, 20976-20992, (2016). PMID: 27510035

30 Wang, J., Pejaver, V. R., Dann, G. P., Wolf, M. Y., Kellis, M., Huang, Y., Garcia, B. A., Radivojac, P. & Kashina, A. Target site specificity and in vivo complexity of the mammalian arginylome. *Sci Rep* **8**, 16177, (2018). PMID: 30385798

31 Crooks, G. E., Hon, G., Chandonia, J. M. & Brenner, S. E. WebLogo: a sequence logo generator. *Genome Res* **14**, 1188-1190, (2004). PMID: 15173120

32 Tan, K., Fujimoto, M., Takii, R., Takaki, E., Hayashida, N. & Nakai, A. Mitochondrial SSBP1 protects cells from proteotoxic stresses by potentiating stress-induced HSF1 transcriptional activity. *Nat Commun* **6**, 6580, (2015). PMID: 25762445

33 Lan X, H. W., Kim SB, Fu D, Abeywansha T, Lou J, Balamurugan U, Kwon YT, Ji CH, Taylor DJ, Zhang Y Oligomerization and a distinct tRNA-binding loop are important regulators of human arginyl-transferase function. *Nature Communications* (under minor revision). PMID:

34 Watanabe, K., Toh, Y., Suto, K., Shimizu, Y., Oka, N., Wada, T. & Tomita, K. Protein-based peptide-bond formation by aminoacyl-tRNA protein transferase. *Nature* **449**, 867-871, (2007). PMID: 17891155

35 Pagani, M., Pilati, S., Bertoli, G., Valsasina, B. & Sitia, R. The C-terminal domain of yeast Ero1p mediates membrane localization and is essential for function. *FEBS Lett* **508**, 117-120, (2001). PMID: 11707280

36 Xu, G., Shin, S. B. & Jaffrey, S. R. Global profiling of protease cleavage sites by chemoselective labeling of protein N-termini. *Proc Natl Acad Sci U S A* **106**, 19310-19315, (2009). PMID: 19892738

37 Long, G. L., Chandra, T., Woo, S. L., Davie, E. W. & Kurachi, K. Complete sequence of the cDNA for human alpha 1-antitrypsin and the gene for the S variant. *Biochemistry* **23**, 4828-4837, (1984). PMID: 6093867

38 Brower, C. S., Piatkov, K. I. & Varshavsky, A. Neurodegeneration-associated protein fragments as short-lived substrates of the N-end rule pathway. *Mol Cell* **50**, 161-171, (2013). PMID: 23499006

39 Zhang, Y., Li, T., Zhang, L., Shangguan, F., Shi, G., Wu, X., Cui, Y., Wang, X., Wang, X., Liu, Y., Lu, B., Wei, T., Wang, C. C. & Wang, L. Targeting the functional interplay between endoplasmic reticulum oxidoreductin-1alpha and protein disulfide isomerase suppresses the progression of cervical cancer. *EBioMedicine* **41**, 408-419, (2019). PMID: 30826359

40 Goitea, V. E. & Hallak, M. E. Calreticulin and Arginylated Calreticulin Have Different Susceptibilities to Proteasomal Degradation. *J Biol Chem* **290**, 16403-16414, (2015). PMID: 25969538

41 Jiang, M., Xie, X., Zhu, X., Jiang, S., Milenkovic, D., Misic, J., Shi, Y., Tandukar, N., Li, X., Atanassov, I., Jenninger, L., Hoberg, E., Albarran-Gutierrez, S., Szilagyi, Z., Macao, B. *et al.* The mitochondrial single-stranded DNA binding protein is essential for initiation of mtDNA replication. *Sci Adv* **7**, (2021). PMID: 34215584

42 Del Dotto, V., Ullah, F., Di Meo, I., Magini, P., Gusic, M., Maresca, A., Caporali, L., Palombo, F., Tagliavini, F., Baugh, E. H., Macao, B., Szilagyi, Z., Peron, C., Gustafson, M. A., Khan, K. *et al.* SSBP1 mutations cause mtDNA depletion underlying a complex optic atrophy disorder. *J Clin Invest* **130**, 108-125, (2020). PMID: 31550240

43 Rai, R. & Kashina, A. Identification of mammalian arginyltransferases that modify a specific subset of protein substrates. *Proc Natl Acad Sci U S A* **102**, 10123-10128, (2005). PMID: 16002466

44 Bachmair, A., Finley, D. & Varshavsky, A. In vivo half-life of a protein is a function of its amino-terminal residue. *Science* **234**, 179-186, (1986). PMID: 3018930

45 Kleifeld, O., Doucet, A., auf dem Keller, U., Prudova, A., Schilling, O., Kainthan, R. K., Starr, A. E., Foster, L. J., Kizhakkedathu, J. N. & Overall, C. M. Isotopic labeling of

terminal amines in complex samples identifies protein N-termini and protease cleavage products. *Nat Biotechnol* **28**, 281-288, (2010). PMID: 20208520

46 Ju, S., Kwon, Y., Kim, J. M., Park, D., Lee, S., Lee, J. W., Hwang, C. S. & Lee, C. iNrich, Rapid and Robust Method to Enrich N-Terminal Proteome in a Highly Multiplexed Platform. *Anal Chem* **92**, 6462-6469, (2020). PMID: 32267142

Arg
Arg
Arg
Arg10
Arg0
1 1
R
R
R
R
R
R
H L
Arg10
Arg0
1 1R
R
H L
662.8701
667.8743
H L
662.8702
663.3719
663.8736
664.3753
664.8769
665.3786
667.8744
668.3760
668.8777
669.3794
669.8811
670.3827
H L
100%
90%
No. pairs

ArginylomePlot

input mzXML results

output

MS1 scans

H/L ratio

MS2 scans

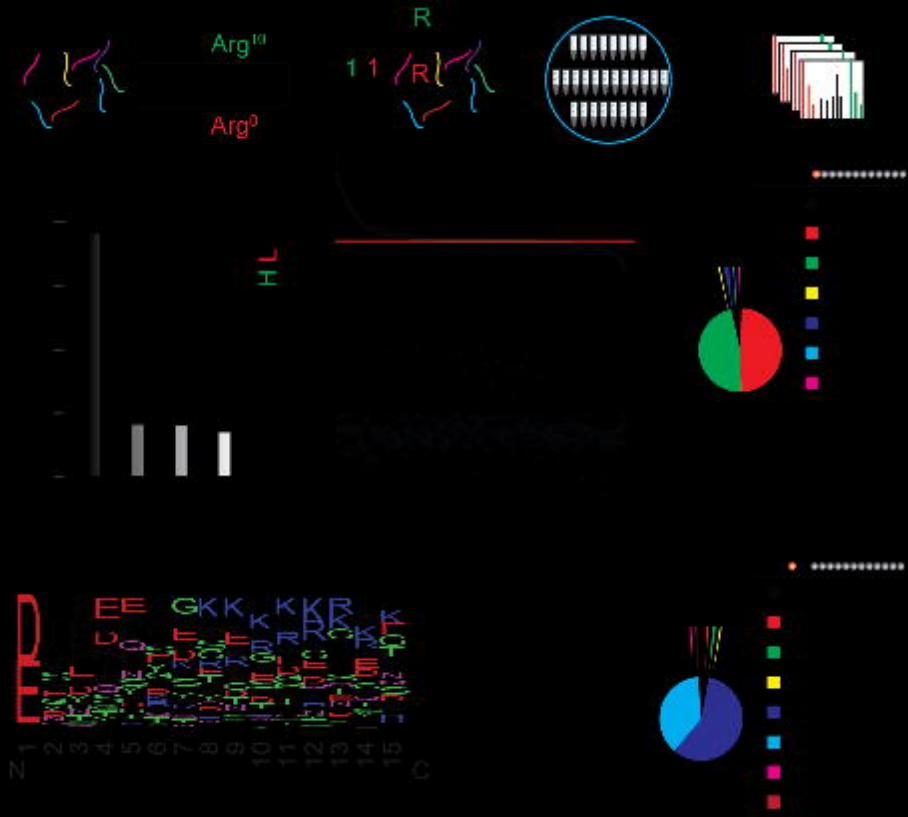

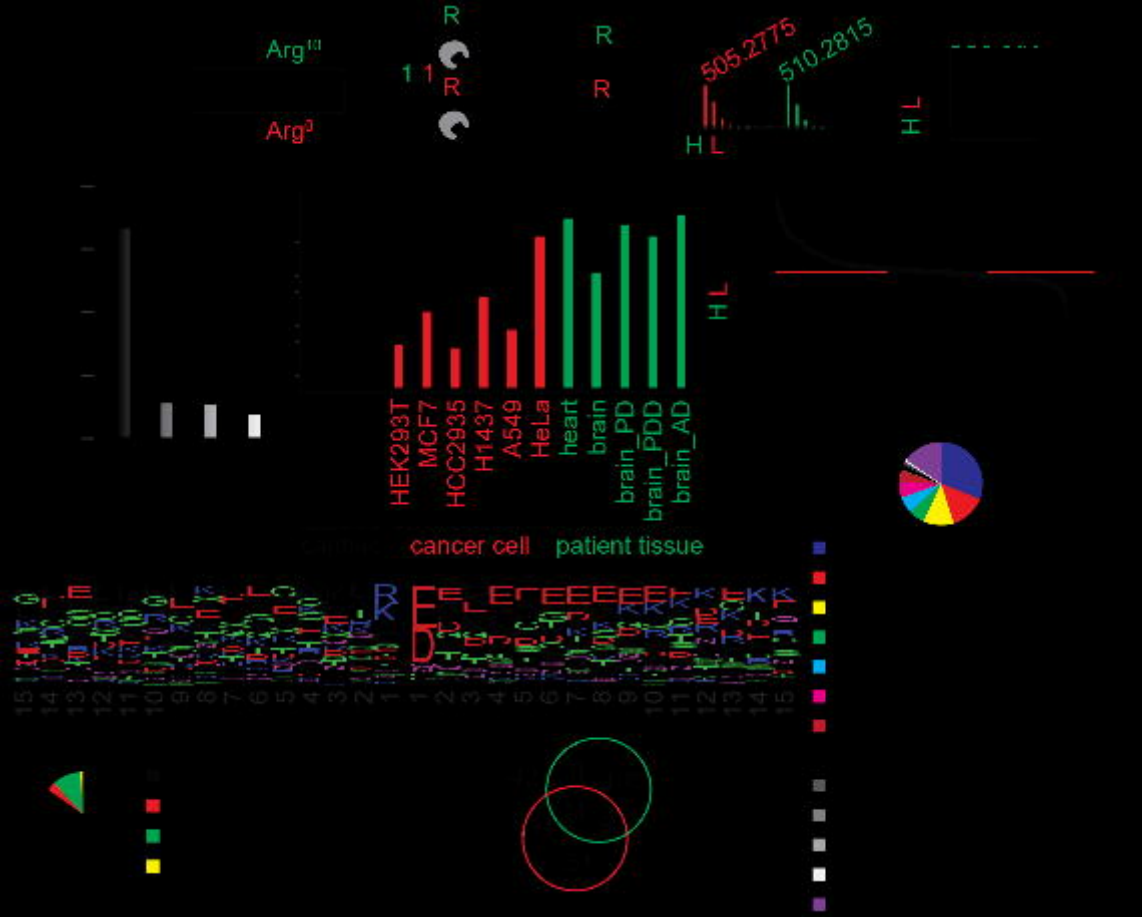
Arg10
Arg3
R
R
R
R
505.2775
510.2815
H L
H L
H L
HEK293T
MCF7
HCC2935
H1437
A549
HeLa
heart
brain
brain_PD
brain_PDD
brain_AD
cancer cell
patient tissue

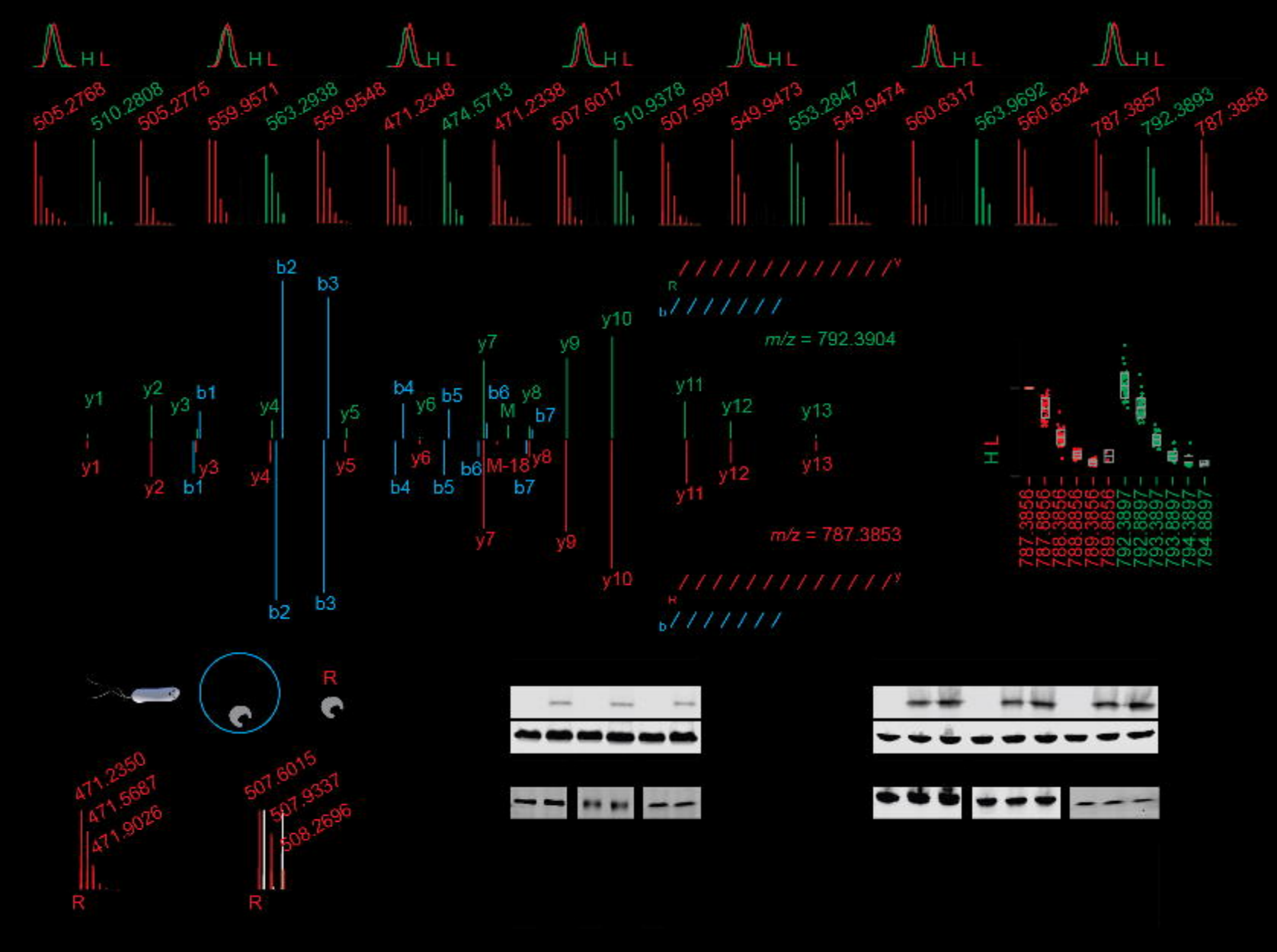
H L
505.2768
510.2808
505.2775
559.9571
563.2938
559.9548
471.2348
474.5713
471.2338
507.6017
510.9378
507.5997
549.9473
553.2847
549.9474
560.6317
563.9692
560.6324
787.3857
792.3893
787.3858
y1
y2
y3
b1
b2
b3
y4
y5
b4
y6
b5
b6
y7
M
y8
b7
M-18
y9
y10
y11
y12
y13
R
m/z = 792.3904
m/z = 787.3853
787.3856
787.8856
788.3856
788.8856
789.3856
789.8856
792.3897
792.8897
793.3897
793.8897
794.3897
794.8897
R
471.2350
471.5687
471.9026
507.6015
507.9337
508.2696

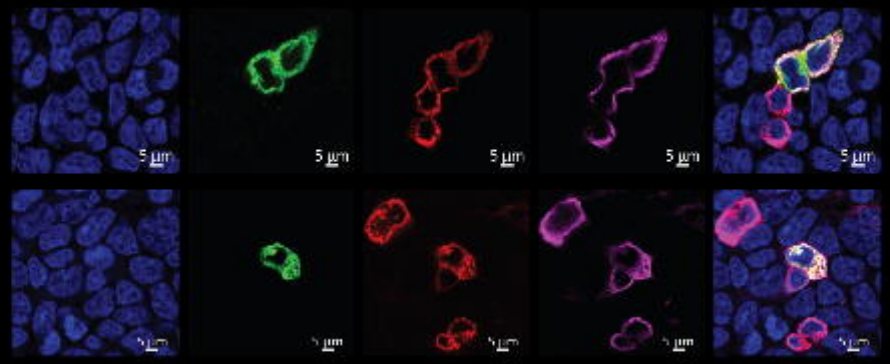

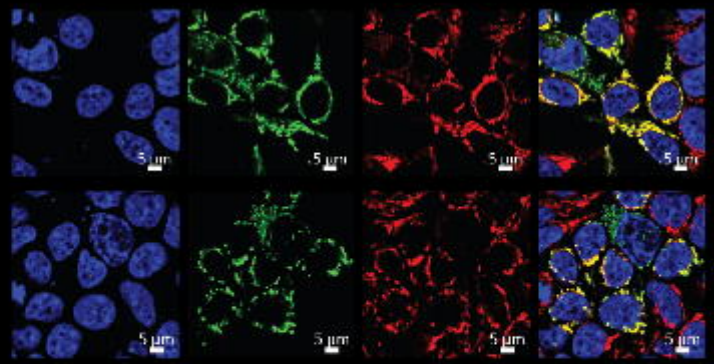

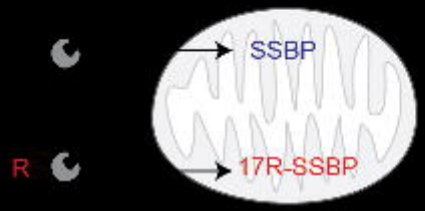

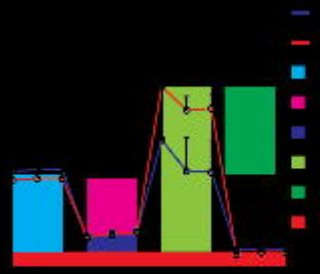

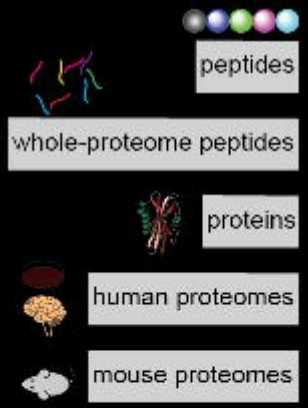

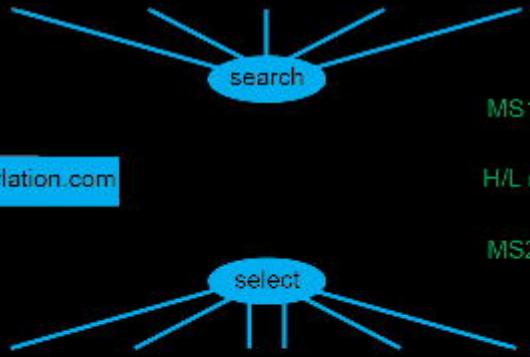

arginylation.com

MS1 spectra

H/L ratio

MS2 spectra

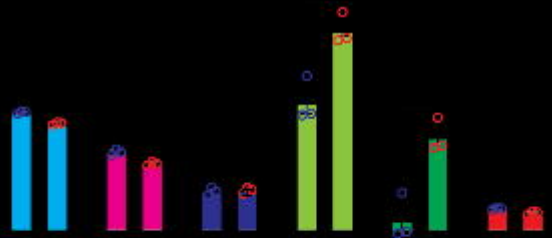

download download